Earth and Planetary Science Letters 510 (2019) 26–36

Contents lists available at ScienceDirect

Earth and Planetary Science Letters

www.elsevier.com/locate/epsl

Temperature fluctuations during the Common Era in subtropical southwestern China inferred from brGDGTs in a remote alpine lake

Xiaoping Feng [a,b,c,d], Cheng Zhao [a,b,*], William J. D'Andrea [c], Jie Liang [d,e], Aifeng Zhou [f], Ji Shen [a]

[a] State Key Laboratory of Lake Science and Environment, Nanjing Institute of Geography and Limnology, Chinese Academy of Sciences, Nanjing 210008, China
[b] Center for Excellence in Quaternary Science and Global Change, Chinese Academy of Sciences, Xi'an 710061, China
[c] Lamont-Doherty Earth Observatory of Columbia University, 61 Route 9W, Palisades, NY 10964, USA
[d] University of Chinese Academy of Sciences, Beijing 100049, China
[e] Key Laboratory of Tibetan Environment Changes and Land Surface Processes, Institute of Tibetan Plateau Research, Chinese Academy of Sciences, Beijing 100101, China
[f] College of Earth and Environmental Sciences, MOE Key Laboratory of Western China's Environmental Systems, Lanzhou University, Lanzhou 730000, China

ARTICLE INFO

Article history:
Received 12 April 2018
Received in revised form 6 November 2018
Accepted 22 December 2018
Available online 17 January 2019
Editor: J. Adkins

Keywords:
lacustrine sediments
brGDGTs
temperature reconstructions
the Common Era
high-elevation region
southwestern China

ABSTRACT

Documenting climate change over the past 2000 years, or the Common Era, is critical to understand how the climate system evolved from one controlled by natural forcings alone to one influenced by anthropogenic greenhouse gas forcing. However, global and regional temperature changes during this interval are still poorly understood, largely due to the limited geographical coverage and scarcity of data. Here we report a well-dated, quantitative, mean annual air temperature (MAAT) record with ~10-yr resolution for the Common Era derived from a sediment core collected at a small alpine lake in remote subtropical southwestern China, and based on a site-specific temporal calibration between down-core analyses of brGDGTs and instrumental data for the interval 1959–2015 AD. The record reveals distinct multicentennial-scale temperature fluctuations, including a relatively cold interval from 0–800 AD, followed by warmer temperatures during the so-called Medieval Climate Anomaly (MCA; 800–1400 AD), cooling during the Little Ice Age (LIA; 1400–1900 AD), and abrupt and rapid warming into the late-20th-century after 1900 AD. Superimposed on these large-scale features are three short-term cold events, centered on 250–310 AD (~0.06 °C), 570–650 AD (~0.87 °C), and 1800–1823 AD (~0.83 °C), respectively. The temperature variations captured in the record are supported by historical documents and existing regional and global paleoclimate records, and correspond in time to a number of the major Chinese dynastic transitions. Importantly, the record captures large-magnitude (up to 4 °C) centennial-scale temperature fluctuations, documents cold conditions during the first millennium AD, and demonstrates that the post-1989 AD warmth is greater than any other time during the past 2000 years. The results suggest that high-elevation areas have been more sensitive than low-elevation regions to climate variations during the Common Era.

© 2018 Elsevier B.V. All rights reserved.

1. Introduction

The past 2000 years, or the Common Era, is an important period during which Earth's climate system has transitioned from being forced solely by natural factors to also being forced by anthropogenic greenhouse gases (IPCC, 2013). To better understand how global and regional-scale climate has changed during this period, the International Past Global Changes (PAGES) project set up the '2k Network' (called PAGES 2k hereafter) in 2009, with the goal of generating a global array of continental-scale temperature reconstructions covering the Common Era. Proxies for past climate, derived from multiple natural archives such as tree rings, corals, ice cores, lake and ocean sediments, as well as historical documents, reveal long-term global cooling during the past millennium, with strong regional differences at decadal- to centennial timescales (PAGES 2k Consortium, 2013). Many of the existing climate records only extend back approximately 1000 years in some continents, including Asia, South America, and Australasia (PAGES 2k Consortium, 2013, 2017). These existing climate records, however, are not evenly distributed in space and time. For instance, records from Asia, South America, and Australasia only extend back approximately 1000 year (PAGES 2k Consortium, 2013, 2017), with climate variations during the first millennium inadequately documented.

* Corresponding author.
E-mail address: czhao@niglas.ac.cn (C. Zhao).

https://doi.org/10.1016/j.epsl.2018.12.028
0012-821X/© 2018 Elsevier B.V. All rights reserved.

Moreover, for some continents like Asia (Cook et al., 2013), about 60% records in PAGES 2k network are based on high-resolution tree-ring data (PAGES 2k Consortium, 2013, 2017), which are not effective recorders of low-frequency multi-centennial scale temperature variability (Moberg et al., 2005; Cook et al., 2013). In particular, the Tibetan Plateau is the most extensive high-elevation area in the world. It has experienced a warming that is double the global average from 1961–2012 AD (Chen et al., 2015), which could potentially influence global atmospheric circulation. Yet temperature changes over the Tibetan Plateau and the surrounding high-elevation areas are under-represented in existing global and continental reconstructions, due to the lack of high quality, quantitative reconstructions.

Branched glycerol dialkyl glycerol tetraethers (brGDGTs), containing two C_{28} alkyl chains with 4–6 methyl substituents and 0–2 cyclopentyl moieties (Fig. S1), are membrane-spanning lipids produced by heterotrophic bacteria, presumed to be members of the phylum Acidobacteria (Weijers et al., 2006; Sinninghe Damsté et al., 2011). Over the last decade brGDGTs have been developed as a proxy for quantitative temperature reconstructions in terrestrial environments. Originally, based on the distribution of nine brGDGTs in a set of globally distributed soil samples, Weijers et al. (2007) demonstrated that the degree of methylation of branched tetraethers (MBT) is correlated with mean annual air temperature (MAAT) and soil pH, while the degree of cyclization of branched tetraethers (CBT) is correlated with pH alone, allowing MAAT to be calculated from combined MBT and CBT measurements. Later, the relationship was modified to exclude two of the GDGTs (IIIb and IIIc) and termed MBT′/CBT (Peterse et al., 2012). Subsequently, brGDGTs have also been examined in lakes, where their distributions are very different from those found in nearby soils, indicating in situ production of brGDGTs in lakes, either in the water column or sediments (e.g., Sinninghe Damsté et al., 2009; Tierney and Russell, 2009; Pearson et al., 2011; Weber et al., 2015; Li et al., 2016). Numerous environmental conditions could potentially impact brGDGT distributions in lakes (Loomis et al., 2014; Dang et al., 2018). Therefore, a number of lake-specific transfer functions between brGDGTs MBT/CBT (or modified forms MBT′/CBT) and MAAT have been determined at both global and regional spatial scales (e.g. Sun et al., 2011; Loomis et al., 2012; Foster et al., 2016; Dang et al., 2018; Russel et al., 2018).

With new developments in chromatography, a new series of structural isomers, novel 6-methyl GDGTs that previously co-eluted with 5-methyl GDGTs, can now be isolated and identified (Fig. S1). These isomers contain branched methyl groups at the α-6/ω-6 position instead of the α-5/ω-5 position (De Jonge et al., 2013). The distribution patterns of 5- and 6-methyl brGDGTs have been examined in soils (e.g. De Jonge et al., 2014a; Naafs et al., 2017a), peats (Naafs et al., 2017b) and lakes (Weber et al., 2015; Russell et al., 2018; Dang et al., 2018). New indices and new methodologies have been proposed to develop calibrations between brGDGTs and MAAT (De Jonge et al., 2014a; Russell et al., 2018). For example, brGDGT-temperature calibration models based on applying a variety of multiple linear regression techniques to brGDGT fractional abundance data from lake sediments have resulted in empirically stronger calibrations with lower prediction error than traditional MBT/CBT indices (e.g. Pearson et al., 2011; Loomis et al., 2012; Foster et al., 2016; Russell et al., 2018). These new developments improve the applicability of brGDGTs for quantitative temperature reconstruction.

Here we report a quantitative temperature record from a sediment core collected from Tiancai Lake, a small alpine lake in southwest China. The 2000-yr long record is based on a site-specific calibration developed by stepwise linear regression between brGDGTs and instrumental data during the regional instrumental period, 1959–2015.

2. Study site

Tiancai Lake (26°38′N, 99°43′E; 3898 m.a.s.l.) is a small alpine lake located in the Hengduan Mountains of Southwestern China, a transitional mountain range between the Tibetan Plateau and the Yunnan–Guizhou Plateau (Fig. 1a). The flow-through lake has a surface area of ∼0.02 km^2, a catchment area of ∼3 km^2, and maximum water depth of 7 m. The freshwater lake is oligotrophic, surrounded by hills rising 200 m above the lake surface (Fig. 1b, c). Bedrock in the catchment is primarily a quartz-poor granitoid (syenite) (Zhang et al., 2017). Forests primarily comprise montane conifers such as *Abies* and *Picea*, which appear undisturbed by human activity (Xiao et al., 2014) and indicate the lake sediment record is also unaffected by human land-use.

The study region is under the influence of the Indian Summer Monsoon and is characterized by strong seasonality (Fig. 1a). During the monsoon season from May to October, the region is hot and humid (Fig. 1d). Instrumental data from the Shangri-la meteorological station (27°30′N, 99°25′12″E; 3277 m.a.s.l.), approximately 110 km southeast of Tiancai Lake, show a mean annual temperature of ∼6.17 °C and a mean annual precipitation of 626.5 mm, with 85% falling during the monsoon season (Fig. 1d).

3. Materials and methods

3.1. Sampling

A 173-cm-long sediment core (TC15A) was collected from the lake center at a water depth of 6.8 m using a piston corer. A parallel 40-cm-long gravity core (TC15C) with well-preserved water-sediment surface was also collected. Both cores were subsampled contiguously at 0.5-cm intervals in the laboratory. In addition, 13 surface sediment samples and 4 soil samples were collected from the lake and surrounding catchment (Fig. 1b). All samples were stored in sterile homogeneous bags at 4 °C until analysis.

3.2. Lipid extraction and brGDGT analysis

Each subsample was freeze-dried, homogenized, and ultrasonically agitated in DCM:methanol (9:1, v:v, 15 min, 4×) for lipid extraction. The total lipid extract was concentrated under a stream of N_2 gas and then saponified at room temperature for 12 h with 6% KOH in methanol solution. The neutral lipids were isolated by liquid–liquid extraction using *n*-hexane (4×) and then separated into apolar and polar fractions (containing GDGTs) by flash chromatography over silica gel (100% activated), using *n*-hexane and methanol, respectively. The polar fractions were filtered through a 0.45 μm PTFE polytetrafluoroethylene filter before analysis.

GDGTs analyses were performed using HPLC-APCI-MS (Agilent 1260 HPLC system with 6100 MS) with auto-injection at the Institute of Tibetan Plateau Research, Chinese Academy of Sciences (ITPCAS). Samples were brought up in 300 μL *n*-hexane: ethyl acetate (EtOA) (84:16, v/v) injection volume was 10 μL. Separation of 5- and 6-methyl brGDGTs isomers was achieved with three Hypersil Gold Silica LC columns in sequence (each 100 mm × 2.1 mm, 1.9 μm, Thermo Fisher Scientific; USA), maintained at 40 °C. GDGTs were eluted isocratically with 84% A and 16% B for the first 5 min, where A = *n*-hexane and B = EtOA, followed by a linear gradient change to 82% A and 18% B from 5 to 65 min and then to 100% B for 21 min, followed by 100% B for 4 min to wash the column and then back to 84% A and 16% B to equilibrate the column. The constant flow rate was 0.2 ml/min throughout. Detection was achieved using positive ion APCI of the eluent. The APCI-MS conditions were set up as follows: nebulizer pressure 60 psi, vaporizer temperature 400 °C, drying gas flow rate 6 L/min and temperature 200 °C, capillary voltage 3500 V, corona 5 μA. Detection was

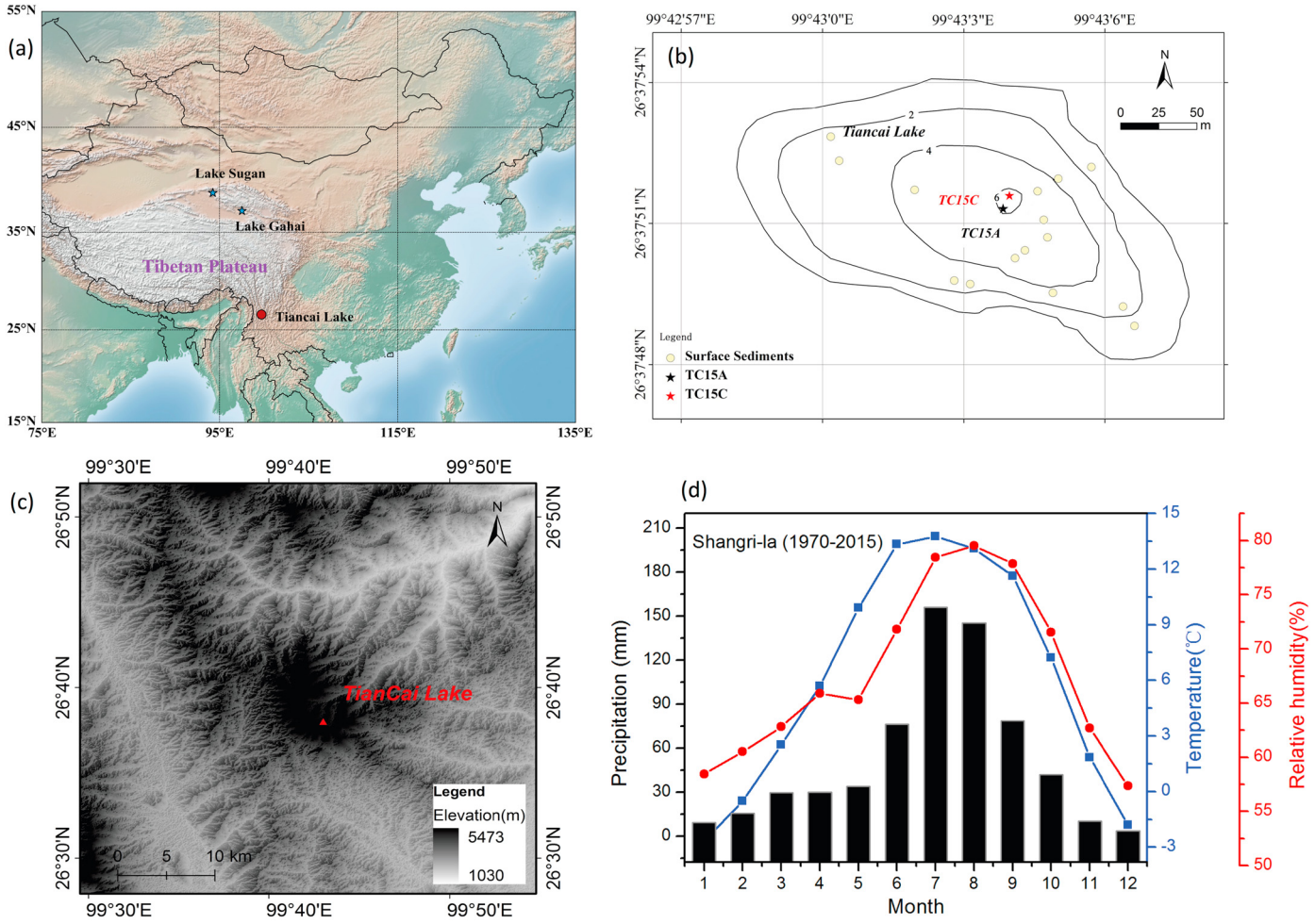

Fig. 1. Location and setting. (a) Location of Tiancai Lake in northwestern Yunnan Province, southwestern China. (b) Lake bathymetry and sampling sites for Tiancai Lake. Red and black stars mark the coring locations of cores TC15C and TC15A, respectively. 2-m contours show lake water depth (m). (c) Shaded DEM showing the topography surrounding Tiancai Lake. (d) Monthly temperature, precipitation, and relative humidity for the period 1970–2015 form the nearby Shangri-la meteorological station. (For interpretation of the colors in the figure(s), the reader is referred to the web version of this article.)

performed in selected ion monitoring (SIM) mode via $[M+H]^+$ at m/z 744 for the C_{46} standard, 1302, 1300, 1298, 1296 and 1292 for the isoGDGTs and 1050, 1048, 1046, 1036, 1034, 1032, 1022, 1020, 1018 for the brGDGTs. We assume the same response factors among different brGDGTs and C_{46} GDGTs. Quantification of GDGTs was achieved by using a lab external standard and integrating the $[M+H]^+$ peak areas manually with the ChemStaion B.04.03 software, assuming an identical response factor for GDGTs. The 5- and 6-methyl brGDGTs were assigned as described by De Jonge et al. (2014b).

3.3. Instrumental data and statistical analyses

To reconstruct quantitative temperature for the past 2000 years, we use a site-specific temporal correlation between sedimentary brGDGT fractional abundance data and instrumental data for the period 1959 to 2015 AD. During this interval, we have samples with ~2-year resolution for use in calibrating brGDGTs with instrumental temperature data. Temperature data are from the Shangri-la meteorological station, ~110 km away from Tiancai Lake, which is the nearest station having similar elevation to Tiancai Lake and uninterrupted data spanning the past 60 years. Because Shangri-la (3277 m.a.s.l.) station is 620 m lower in elevation than Tiancai Lake, we apply a lapse rate of ~0.58 °C /100 m based on local meteorological data from nearby weather stations (Shangri-la and Jianchuan station) to adjust the temperature dataset to represent Tiancai Lake's elevation. To account for chronological uncertainties in our calibration-in-time, a 3-year moving average of the instrumental MAAT was used.

We compute the Pearson correlation matrix with significance levels (p value) between the fractional abundance ($f(i)$) of each individual brGDGT and MAAT for the calibration interval using the ggcorrplot package (Kassambara, 2016). For $f(i)$, we consider the standard deviation of the fractional abundance of each brGDGTs from the average duplicate error (0.002). We also calculate the 2-sigma uncertainties of inferred MAAT by propagating the standard deviation of each $f(i)$ using the error transfer formula based on the site-specific temporal calibration. The compound structures of all brGDGTs examined in this study are shown in Fig. S1, and values for various indices are reported in Table S1 (see details in supplementary materials).

4. Results

4.1. Chronology

The chronology of core TC15A was established using 5 AMS-^{14}C radiocarbon dates on terrestrial plant fragments (Beta Analytic Testing Laboratory) (Fig. 2a). All ^{14}C dates were calibrated to calendar years with the program CALIB 7.1 using the IntCal 13 calibration data set (Reimer et al., 2013). ^{210}Pb and ^{137}Cs were analyzed at 0.5-cm intervals in core TC15C using a gamma spectrometer (Hyperpure Ge detector) at State Key Laboratory of Lake Science and Environment, Nanjing Institute of Geography and Limnology,

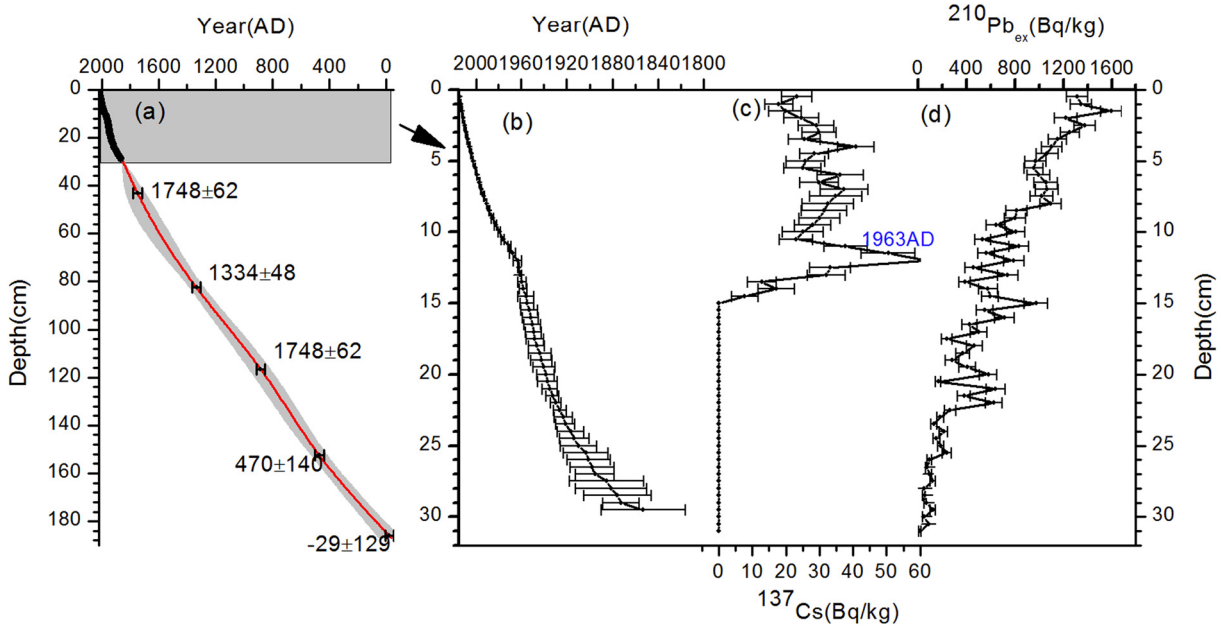

Fig. 2. ^{137}Cs (c) and $^{210}Pb_{ex}$ (d) activity concentrations (Bq/kg) in Tiancai Lake short core TC15C. A composite age model for the sediments (a) was developed using $^{210}Pb_{ex}$ and ^{137}Cs results (b) from core TC15C and five radiocarbon dates on plant remains from core TC15A. Vertical profile of ^{210}Pbex (= $^{210}Pb_{total}$–^{226}Ra) in sediment core decreased exponentially.

Chinese Academy of Science (Fig. 2c, d). Total ^{210}Pb activity decreases exponentially with depth and stabilizes at 31 cm (Fig. 2d). The ^{137}Cs peak appears at 12 cm depth and corresponds to the year 1963 AD (Fig. 2c), which had the most extensive worldwide nuclear weapon testing (Appleby, 2002). The age model of core TC15C was constructed using the constant rate of supply (CRS) model combined with a constant initial concentration (CIC) model and using the ^{137}Cs peak as a fixed time marker (Appleby, 2002) (Fig. 2b). A composite age model for the sediments was developed using both ^{210}Pb analyses from core TC15C and radiocarbon dates on TC15A using the Bacon program (Blaauw and Christen, 2011) (Fig. 2a).

4.2. Modern brGDGT distributions and brGDGT-temperature calibration

5- and 6-methyl brGDGTs in all lake sediment and catchment soil samples were chromatographically separated, and non-cyclopentane moieties are predominant in each sample (Fig. 3a, b, c). In lake surface sediments, pentamethylated brGDGTs are generally the most abundant (45.2%), followed by hexamethylated brGDGTs (33.9%) and tetramethylated brGDGTs (21.0%). In soil samples, tetramethylated brGDGTs (46.6%) are the most abundant, followed by pentamethylated (44.1%) and hexamethylated brGDGTs (8.8%) brGDGTs (Fig. 3c). The relative amount of cyclopentane ring-containing brGDGTs in sediments and soil samples is generally low and sometimes too low to be detected and integrated reliably, especially the 5- and 6-methyl isomers IIIb, IIIc and IIc. In both groups, the 5-methyl brGDGTs are the most abundant isomers, contributing 81% and 96% of the total amounts of brGDGTs in Tiancai Lake surface sediments and soils, respectively (Fig. 3d). The ratio of 6-methyl brGDGTs to 5-methyl GDGTs (IR_{6me}) varies between 0.04 and 0.10 in the catchments soils, and between 0.21 and 0.30 in surface sediments.

The calculated site-specific temporal calibration function is as follows, and was applied to down-core sediments to develop the temperature reconstructions for the Common Era:

$$MAAT = 14.74 - 34.46 \times f(IIIa) + 27.49 \times f(IIa) - 35.36 \times f(IIb) - 60.36 \times f(Ia) - 95.91 \times f(Ib) \quad (1)$$

$$\left(r^2 = 0.93,\ \mathrm{RMSE} = 0.18\,^{\circ}\mathrm{C},\ n = 27\right) \quad (2)$$

4.3. Temperature changes at Tiancai Lake during the Common Era

As shown in Fig. 5a, the brGDGT-inferred MAAT record from Tiancai Lake has an average sampling resolution of 10 years, and indicates that MAAT varied between −0.2 ± 0.5 °C and 3.8 ± 0.5 °C during the past 2000 years. Reconstructed MAAT generally varies from 0 and 2 °C at multi-centennial scales from 0 to 800 AD, with two distinct low temperature intervals centered at 250–310 AD and 570–650 AD, respectively. From 800–1400 AD, inferred-MAAT warmed to between 2 and 3 °C and exhibited modest decadal- and centennial-scale fluctuations. From 1400 to 1800 AD, inferred-MAAT gradually decreased toward a low value of 0 °C, and then increased by 1.6 °C until 1900 AD. After a slight temperature decrease of 0.6 °C between 1900 and 1950 AD, MAAT rose abruptly to the present day (from 1.1 to 3.8 °C).

5. Discussion

5.1. brGDGT distributions and site-specific brGDGT-MAAT calibration for Tiancai Lake

Our analysis of modern samples reveals different brGDGT distribution patterns between surface sediments and soil samples, with IIa and IIIa dominating in surface sediments and Ia and IIa dominating in catchment soils (Fig. 3a). The different distributions indicate the majority of brGDGTs in sediments of Tiancai Lake are likely produced within the water column rather than transported from catchment soils, as has also been inferred in previous studies (Tierney and Russell, 2009; Sinninghe Damsté et al., 2009; Weber et al., 2015; Dang et al., 2018; Russell et al., 2018). We also compare the fractional abundances of summed tetra-, penta- and hexamethylated brGDGTs between Tiancai Lake and other sample sets analyzed by the new analytical method, including lake sediments in East African lakes (Russell et al., 2018), global soils (De Jonge et al., 2014a), and global peats (Naafs et al., 2017b) spanning the MAAT range of the Tiancai Lake calibration (0–5 °C) (Fig. 3e) and for the full MAAT range of all of the calibration datasets

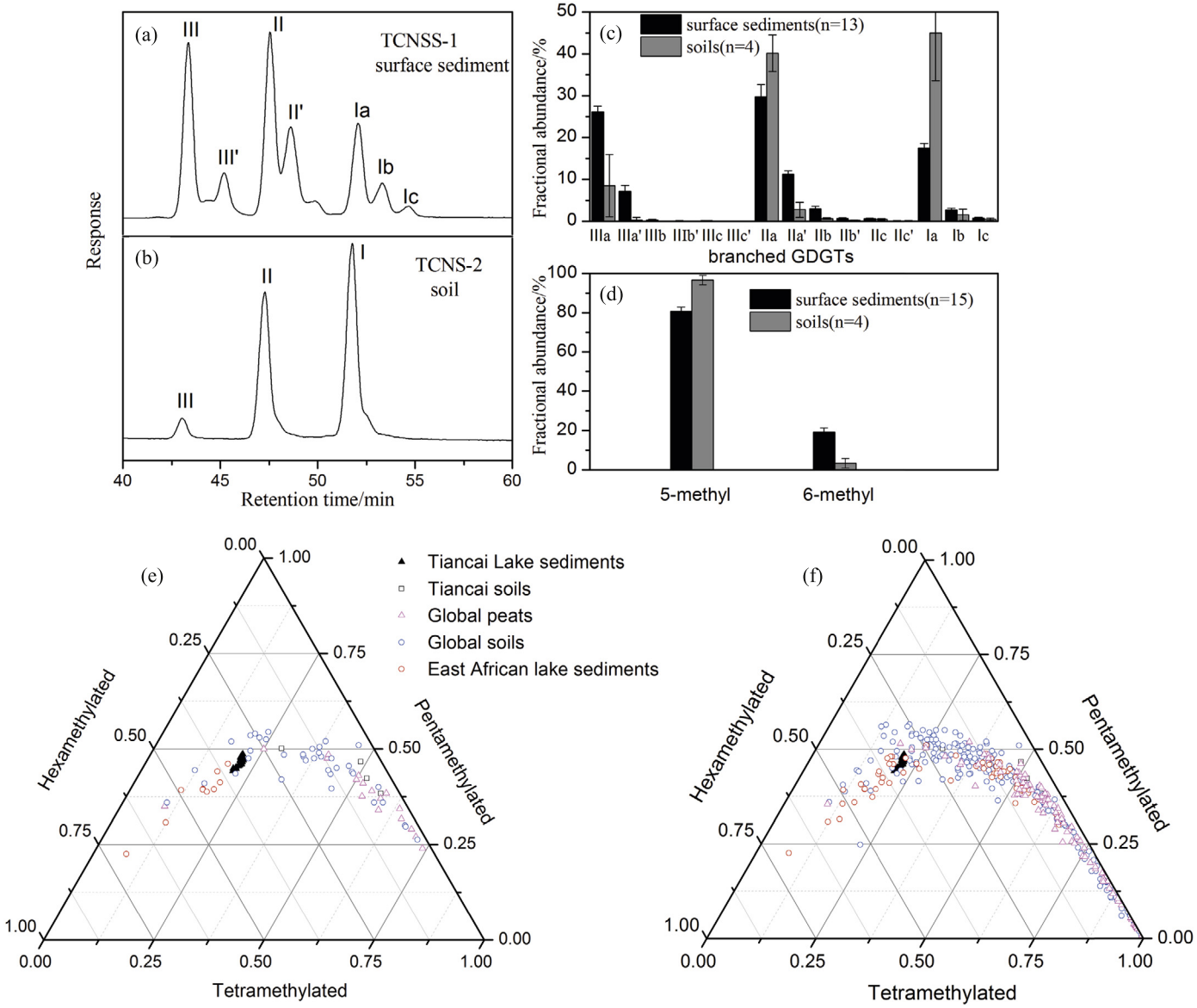

Fig. 3. HPLC–APCI/MS base peak chromatograms for typical (a) lake surface sediment samples and (b) soil from Tiancai Lake catchment. (c) Average fractional abundance of brGDGTs in lake surface sediments (black columns) and surrounding soil samples (gray columns) of Tiancai Lake. (d) Proportion of 5-methyl and 6-methyl branched tetraethers relative to total brGDGTs in lake surface sediments (black columns) and soils (gray columns). (e) The fractional abundances of tetramethylated, pentamethylated, and hexamethylated brGDGTs in Tiancai Lake down-core sediments and modern soils, together with those from globally distributed peat deposits (Naafs et al., 2017b), globally distributed soils (De Jonge et al., 2014a), and East African lakes (Russell et al., 2018) restricted to the temperature range (0–5 °C) of the Tiancai Lake calibration and (f) for the full temperature range of all calibrations (−8.3–26.8 °C).

(−8.3–26.8 °C) (Fig. 3f). Within the restricted temperature range of the Tiancai Lake calibration (Fig. 3e; 0–5 °C), the East African lacustrine data (Russell et al., 2018) exhibit dominance of penta- and hexamethylated brGDGTs over the tetramethylated brGDGTs (as is observed in Tiancai Lake sediments) while the global soils and peats data (De Jonge et al., 2014a; Naafs et al., 2017b) and Tiancai surface soils data exhibit a greater range of variability in brGDGT distributions and contain greater proportions of tetramethylated brGDGTs. This once again highlights the differences in brGDGT distributions between lacustrine sediments and soils and peats.

The reconstructed temperature trends and absolute values calculated using previously published site-specific brGDGTs-temperature calibrations (e.g., Tierney et al., 2010; Sun et al., 2011; Loomis et al., 2012; Günther et al., 2014; Dang et al., 2018; Russell et al., 2018) did not correlate well with instrumental or proxy temperature records from the region (Figs. S2, S3), highlighting the need for site-specific calibration. In addition, temperatures reconstructed from Tiancai Lake for the past ~60 years using the existing calibrations do not even exhibit the general warming trend clearly observed in instrumental data (see details in supplementary materials).

To further examine the relation between individual brGDGT compounds and temperatures, we perform Pearson correlations between fractional abundances of major brGDGT compounds (IIIa, IIIa′, IIa, IIa′, IIb, IIb′, Ia, Ib, Ic) and MAAT in different sample sets, including the down-core sediments of Tiancai Lake spanning 1959–2015 AD, East African lakes (Russell et al., 2018), global soils (De Jonge et al., 2014a), and global peats (Naafs et al., 2017b) (Fig. 4). The results show that IIIa and Ia are negatively correlated to MAAT with strong statistical significance ($r = -0.85$, -0.84, respectively; $p < 0.0001$) in Tiancai Lake, whereas IIb is positively correlated to MAAT with strong statistical significance ($r = 0.89$; $p < 0.0001$) (Fig. 4a). We include this analysis here to highlight the fact that the fractional abundance of any particular brGDGT can be

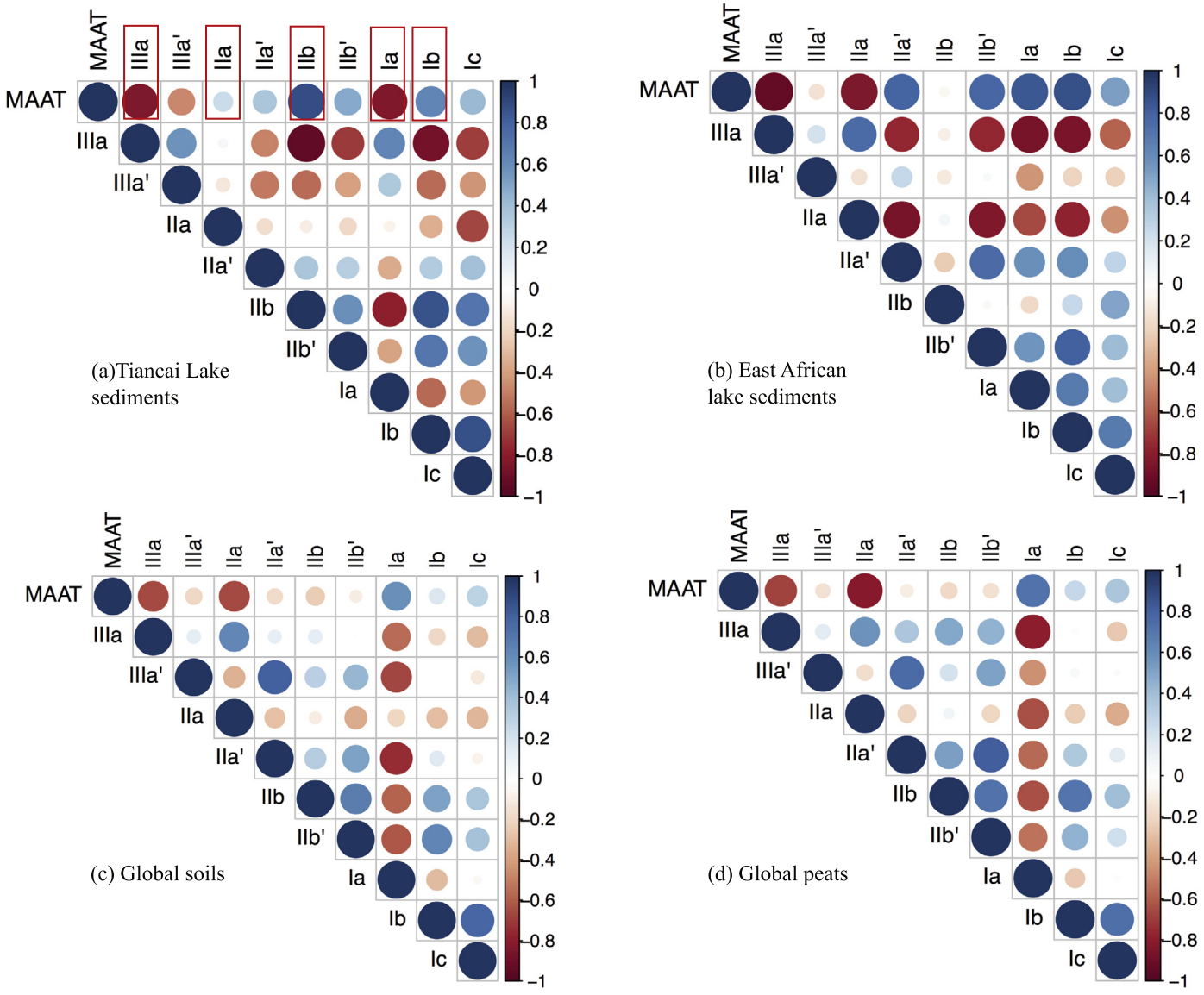

Fig. 4. Pearson correlation matrix for (a) the down-core brGDGT fractional abundance data across the instrumental period, (b) East African lake surface sediments (Russell et al., 2018), (c) globally distributed soils (De Jonge et al., 2014a), and (d) globally distributed peat samples (Naafs et al., 2017b) with MAAT. Positive correlations are blue and negative correlations are red. Color intensity and symbol size are proportional to the correlation coefficients.

positively correlated to temperature in one calibration set, while negatively correlated in another (Fig. 4b, c, d). In particular, the strong negative correlation between IIIa, Ia and MAAT and weak positive correlation between IIa and MAAT at Tiancai Lake might be the cause for calculated temperature biases based on existing calibration functions. In addition, many of these existing functions are based on analytical methods that did not separate 5-me and 6-me brGDGTs, potentially leading to additional uncertainties when applied to data sets wherein these compounds are resolved. Moreover, calibration functions based on global sample sets may not be appropriate for application to specific sites due to specific environmental constraints on brGDGTs, varying proportions of lacustrine versus soil contributions at different sites, as well as the potential input from different bacterial taxa (e.g. Tierney and Russell, 2009; Foster et al., 2016; Russell et al., 2018).

To develop a site-specific brGDGT-temperature calibration that minimizes prediction errors, we perform stepwise forward selection (SFS) regression between down-core brGDGT results and instrumental MAAT over the period 1959–2015 AD (Hocking, 1976). We also note some concerns when applying even site-specific brGDGT-based temperature calibrations for long-term MAAT reconstructions. First, although lacustrine brGDGTs dominate the Tiancai Lake sediments, we cannot exclude the influences of brDGDTs produced in soils. However, because brGDGTs in surface sediments do not show any correlation with water depth (Fig. S2), we infer minimum contributions from soil-derived brGDGTs, which, if present, we would expect to be greater in littoral than profundal sediments. Second, the BIT index, an indicator of changes in depositional environment (Sinninghe Damsté et al., 2009), shows stable and high values in lake surface sediments and in sediment core samples (Fig. 5b), suggesting a stable depositional environment throughout the past 2000 years. Therefore, we find it reasonable to apply the calibration derived from the past 60 years to the entire 2000-year sediment record. Third, our calibration is based on air temperature rather than water temperature, which could introduce uncertainties, especially considering that the dominating brGDGTs are produced within lakes. Unfortunately, we do not have continuous water temperature data for this remote lake. However, previous studies using large datasets have shown that air temperatures generally correspond to lake surface water temperature

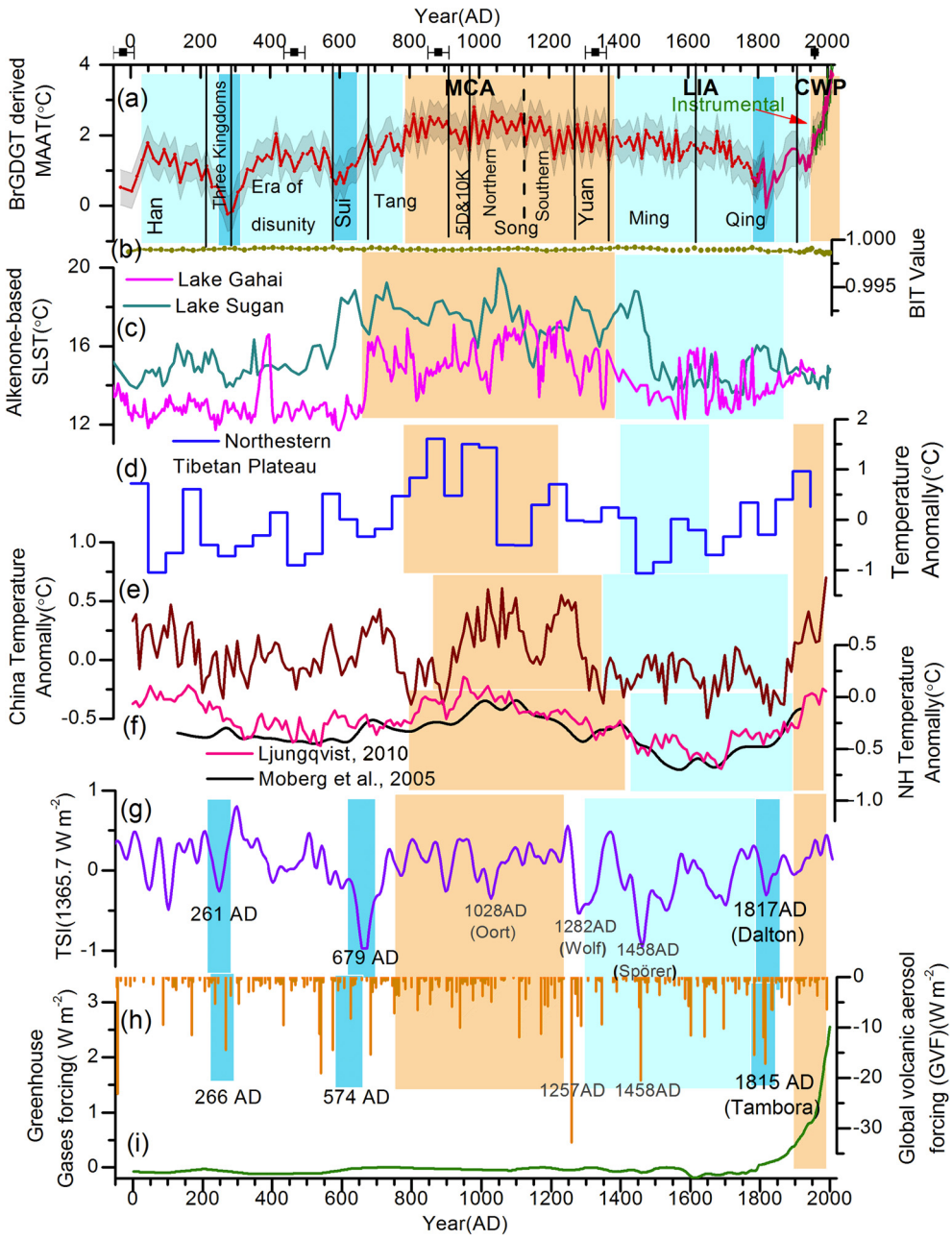

Fig. 5. Proxy-inferred temperature fluctuations and forcing factors during the Common Era. (a) brGDGT-inferred MAAT reconstruction (red line) with $\pm 2\sigma$ uncertainty (gray shaded area) for the past 2000 years based on the site-specific brGDGT-temperature calibration model (this study). Lapse rate-adjusted instrumental temperature in green for the interval 1959–2015 AD. The cyan shaded areas indicate cold periods, and the yellow shaded areas indicate warm intervals. The blue vertical bars denote the three cold events. Chinese dynasties are indicated, as are the Five Dynasties Period (5D) and Ten Kingdoms Period (10K); (b) Down-core BIT index from core TC15A; (c) Alkenone-inferred summer lake surface temperature (SLST) records from Lake Sugan and Lake Gahai (He et al., 2013) on the Tibetan Plateau; (d) 50-year average temperature anomalies from the northeastern Tibetan Plateau derived from multi-proxy data (Yang et al., 2003); (e) Composite temperature anomalies from China based on numerous proxy-based studies (Ge et al., 2013a); (f) Composite temperature anomalies for the Northern Hemisphere (Moberg et al., 2005; Ljungqvist, 2010); (g) Total Solar Irradiance (TSI) (Steinhilber et al., 2012); (h) Global volcanic aerosol forcing (Sigl et al., 2015); (i) Greenhouse gas forcing (Crowley, 2000).

(Dieffenbacher-Krall et al., 2007; Russell et al., 2018). Considering the small volume of this shallow, flow-through lake, changes in lake water temperature likely responds quickly to air temperature changes. Therefore, we argue that our site-specific brGDGT-based temperature calibration is appropriate for MAAT reconstructions over the past 2000 years at Tiancai Lake.

5.2. brGDGT-inferred temperatures during the Common Era

The inferred-MAAT record from Tiancai Lake reveals multicentennial-scale variations between 0 °C and 4 °C during the Common Era (Fig. 5a). Specifically, our data indicate a relatively cold period from 0–800 AD with two distinct multicentenial-scale cold events centered on 250–310 AD and 570–650 AD, during which time MAATs were near 0 °C. A warm period with temperatures around 2–3 °C at 800–1400 AD likely corresponds to the so-called Medieval Climate Anomaly (MCA) (Jones and Mann, 2004). The cooling interval between 1400 and 1900 AD, with the coldest temperatures (0 °C) ca. 1800 AD, probably corresponds to the well-documented Little Ice Age (LIA) (Jones and Mann, 2004). After a 0.6 °C cool perturbation between 1900 and 1950 AD, the temperature record indicates an abrupt 2.7 °C warming until present, i.e., the well-known late-20th-century warming. In particular, post-

1989 warmth, captured in both the brGDGT-inferred temperature record and instrumental record, is greater than at any other time during the past 2000 years.

Recently, a few studies have linked climatic changes and social developments in ancient China by comparing paleoclimate records with historical records of dynastic transition (Zhang et al., 2010 and references therein). The Tiancai Lake temperature record is supported by historical documents concerning climate conditions during successions of Chinese dynasties in the Common Era (Fig. 5a). A relatively cold climate was documented during the 1st to the 6th Centuries AD, corresponding to the Eastern Han Dynasty, Three Kingdoms, Wei, Jin Dynasties and Southern and Northern Dynasties (The Era of disunity Dynasty) (Chu, 1973) during which time the Tiancai Lake record also indicates cold temperatures (averaged 1.15 ± 0.5 °C). Furthermore, the two cold episodes observed in our record, centered at 250–310 AD (0.06 ± 0.5 °C) and 570–650 AD (~0.87 °C ± 0.5 °C), correspond with documented cold periods that marked dynastic transitions near the end of the Three Kingdoms Dynasty at 280 AD, and at the transition from the Jin Disunity to the Southern and Northern Dynasties (Chu, 1973) (Fig. 5a). After the 570–650 AD cold event, the temperature became warm (averaged 2.04 ± 0.5 °C) during the Tang–Song–Yuan Dynasties, which were times of great prosperity (Chu, 1973), corresponding with the warmth of the MCA captured in the Tiancai Lake record. Decreasing temperatures during the LIA (averaged 1.36 ± 0.5 °C) corresponded with the Ming-Qing cold period (Ge et al., 2013b). In particular, the coldest interval (0.83 ± 0.5 °C) of the LIA recorded at Tiancai Lake, ca. 1800–1823 AD, corresponds to a period of widespread starvation in the Yunnan region, attributed to consecutive years (from 1815 to 1817) with extremely cold summers and autumns (Yang, 2005).

Considering the role of natural climate variations can help develop a more holistic view of the factors that have influenced human history. Although climate is not the only factor that influences society, especially in a complex and advanced society such as dynastic China, it is undoubtedly an important one. Consecutive years with cold growing seasons can lead to food shortages, resulting in famine, more social conflicts and warfare, and can potentially contribute to dynastic transitions (Zhang et al., 2005). It is worth noting that unlike composite temperature data from the central and eastern Tibetan Plateau, and northwest, eastern, and northeastern China, our new record represents a site remote from northern pastoral nomadic regions and is less likely to have been influenced by human activities. Previous studies have proposed that the collapse of agricultural dynasties of the Han, Tang, Song and Ming were related to periods of cold temperature (Zhang et al., 2010). Our record also generally reveals low temperatures, or rapid decline of temperature, corresponding to these major dynastic collapses (Fig. 5a). The observed connections between major climate changes and social transitions point toward the influence of climate variability on the history of China during the Common Era.

5.3. Coherent variations in regional and hemispheric temperature history

Our record is similar to broader regional temperature reconstructions from East Asia and the average Northern Hemisphere. For instance, alkenone-based lake water temperature reconstructions at both Sugan and Gahai Lakes in the arid northern Tibetan Plateau show colder conditions prior to ~600–700 AD, a warm MCA between 700–1400 AD, and cooling during the ensuing LIA (Fig. 5c; He et al., 2013). Similarly, tree-ring based temperature reconstructions in the northeastern Tibetan Plateau show the same temperature trends during the Common Era (Fig. 5d; Yang et al., 2003), as does a recent synthesis of temperature changes in China (Fig. 5e; Ge et al., 2013a). Similar multicentennial-scale variations have been documented in temperature reconstructions for the Northern Hemisphere (Fig. 5f; Moberg et al., 2005; Ljungqvist, 2010). However, the timing and amplitude of these multicentennial-scale intervals of relative warmth and cooling, such as the MCA and LIA show differences among various records, potentially due to chronological uncertainties and differing proxy sensitivities among the records. In particular, the coldest interval of the LIA at Tiancai Lake occurred in the early 19th century, which is later than what is reported for other records, including the inferred-temperature records from Lake Sugan and Lake Gahai (Fig. 5c), and reconstructed temperature anomalies over the northeastern Tibetan Plateau, China, and the Northern Hemisphere in aggregate (Fig. 5d–f), as well as for Europe; however, the LIA timing at Tiancai Lake is in close agreement with records from the Arctic and North America (PAGES 2k Consortium, 2013). These temporal and spatial differences in temperature changes during the MCA and LIA probably reflect differential regional responses to broader-scale climate anomalies (Yang et al., 2003; Mann et al., 2009; Diaz et al., 2011; IPCC, 2013; Shi et al., 2015).

Our data show an abrupt warming trend starting at the end of LIA, with the most rapid warming occurring after 1950 AD. The Tiancai Lake record indicates that the last 25 years (1989 to 2015 AD) was the warmest interval of the past two millennia, 1 °C warmer than even the MCA. This result is supported by the recent IPCC report, which suggests that average annual temperatures in the Northern Hemisphere from 1982 to 2012 AD are very likely the warmest 30 years of the last 800 years (high confidence), and probably the warmest of the last 1400 years (medium confidence) (IPCC, 2013). PAGES 2k reported warming across all seven continents since the end of the 19th century (PAGES 2k Consortium, 2013). Similar findings have been reported for China and Asia (Ge et al., 2013a; Shi et al., 2015). Indeed, the Tiancai Lake record indicates that the current warming is unprecedented for the entire Common Era.

Another interesting feature in the Tiancai Lake record is the relatively cold climate during most of the first millennium. Although temperature syntheses spanning the past 2000 years exist for the Arctic, Europe, and Antarctic, they only extend back to ~800 AD in Asia (PAGES 2k Consortium, 2013). Furthermore, even during the past 1000 years, there are large uncertainties in the MAAT reconstruction in China prior to the 16th century, due to complications in the dating methods and proxy calibrations and sensitivities (Ge et al., 2013b). However, a cold first millennium has been documented in certain published records, including the alkenone-based temperature records from Sugan and Gahai Lakes (Fig. 5c; He et al., 2013), as well as tree-ring based temperature reconstructions in the northeastern Tibetan Plateau (Fig. 5d; Yang et al., 2003). In addition, the synthesized temperature anomalies in China and the Northern Hemisphere show slightly cooler temperatures during most of the first millennium (Fig. 5e, f; Moberg et al., 2005; Ljungqvist, 2010; Ge et al., 2013a). Considering the different amplitude of cooling between temperature records around the Tibetan Plateau and data from other areas, we hypothesize that the first millennium cooling could be a regional climate pattern in high-altitude areas around the Tibetan Plateau.

It is worth pointing out that our record displays more than 4 °C of variability in MAAT during the Common Era, including ~3 °C variability during the preindustrial period and more than 2 °C during post-industrial warming. In comparison, regional temperature syntheses show about 1 °C preindustrial variations in China (Fig. 5e; Ge et al., 2013a), and preindustrial variations of less than 1 °C in the Northern Hemisphere (Fig. 5f; Moberg et al., 2005; Ljungqvist, 2010). During the LIA, the Tiancai Lake record indicates a ~2 °C MAAT decrease, while the Northern Hemisphere average temperature decrease in the LIA is approximately 1 °C

(Fig. 5f; Moberg et al., 2005; Ljungqvist, 2010). Interestingly, the tree-ring based temperature reconstruction at the northeastern Tibetan Plateau also show ~3 °C variations for preindustrial periods, about twice that for China as a whole (Fig. 5d). Indeed, the recent warming at Tiancai Lake recorded by instrumental data shows an average warming rate of about 0.4 °C per decade from 1960 to 2015, which is similar to the warming rate (0.316 °C/decade) observed in instrumental data over the Tibetan Plateau from 1961 to 2012 (Yan and Liu, 2014). This warming rate is approximately twice that of the average warming across China (Chen et al., 2015). The relatively large amplitude temperature variations over the Tibetan Plateau and surrounding high elevation regions likely represent amplified temperature sensitivity in high elevation regions (Pepin et al., 2015).

5.4. Climate forcing in high elevation regions

The multicentennial-scale temperature fluctuations during the Common Era documented in the Tiancai Lake record, including the general cold interval in the first millennium, the warm MCA, and cold LIA, are potentially related to centennial-scale variations in solar activity and volcanic eruptions (Fig. 5g, h). Total solar irradiance (TSI), which is computed from ^{10}Be records in ice cores and ^{14}C records in tree-rings (Steinhilber et al., 2012), shows generally lower background levels with distinct decadal- to centennial-scale minima during the first millennium and the LIA, and higher background levels during the MCA (Fig. 5g). A reconstruction of global volcanic aerosol forcing suggests there were more eruptions during the first millennium and during the LIA, and fewer eruptions during the MCA (Fig. 5h; Sigl et al., 2015). In particular, the three distinct cold intervals at 250–310 AD, 570–650 AD, and 1800–1823 AD in the Tiancai Lake record coincide within dating uncertainties with both solar minima (centered at 261 AD, 679 AD and 1817 AD (Dalton)) and strong volcanic eruptions (266 AD, 574 AD and 1815 AD) (Fig. 5g, h). The ~1815 AD eruption is located in Tambora/Indonesia and close to our site. Of course, solar activity and volcanic eruptions have been proposed as the primary forcing for climate variations at decadal and centennial scales over the Common Era (Crowley, 2000; PAGES 2k Consortium, 2013), and have been implicated in inferred climate perturbations in various regions, including the Tibetan Plateau (e.g. He et al., 2013), East Asia (e.g. Cook et al., 2013), North and Central America (e.g. Gennaretti et al., 2014), Europe (e.g. Hegerl et al., 2011), and the Arctic (e.g. Wiles et al., 2004). We note that not all reconstructed solar minima and/or volcanic eruptions correspond with cold temperatures in our record. For example, our data show no temperature decease during the solar minima of 1028 AD, 1282 AD, and 1458 AD (Fig. 5g), nor during the strong volcanic eruptions at 540 AD, 1257AD and 1458 AD (Fig. 5h).

The abrupt temperature rise of recent times is likely due to increases in greenhouse gases (GHGs) (Fig. 5i), as noted in numerous other climate studies (IPCC, 2013). It has recently been argued, based on observational data, that high-elevation regions experienced more rapid postindustrial warming than lower-elevation regions (e.g., Liu and Chen, 2000; Li et al., 2011; Wang et al., 2014). The quantitative temperature reconstruction from Tiancai Lake provides observational evidence from the geologic record that centennial-scale temperature fluctuations during the Common Era were also amplified at high elevation regions. Multiple factors could help explain the greater temperature sensitivity in high-elevation regions. For low-latitude regions, the elevation-dependent snow cover duration and resulting albedo feedbacks would induce non-linear responses of the surface absorption of incoming solar radiation, which could be a major factor for high-elevation regions (Pepin et al., 2015 and references therein). Similar changes in albedo related feedbacks such as the ratio of snow to rain and the migration of the treeline are also important in the Tibetan Plateau and Himalaya regions (Pepin et al., 2015 and references therein). Also, changes in cloud cover and cloud properties could affect radiation and thus surface energy budget, and would be more variable in high-elevation areas thus inducing larger temperature changes (Yan and Liu, 2014 and references therein). Other factors, including water vapor- and aerosol-radiative feedbacks could contribute to different climate sensitivities at different elevations (Rangwala et al., 2009; Lau et al., 2010). However, due to limited observations from high elevation regions, the exact mechanisms responsible for amplification of temperature variability at higher elevations need further investigation through a combination of observational analyses and modeling studies.

6. Conclusions

A decadally resolved, quantitative, brGDGT inferred-MAAT record from Tiancai Lake reveals major multicentennial-scale temperature fluctuations for the Common Era in low-latitude, high-elevation southwestern China. The major features of the temperature history inferred from this record include a relatively cold first millennium, a warm period coincident with the Medieval Climate Anomaly (800–1400 AD), a cold period during the Little Ice Age (1400–1900 AD) that culminated toward the end of this period (~1825 AD), and rapid warming into the Current Warm Period. Three discrete cold events, centered on 250–310 AD, 570–650 AD, and 1800–1823 AD, are also observed. A number of transitions between major Chinese dynasties coincide with intervals of low temperature or rapidly declining temperature, providing additional evidence that natural climate variations influenced the human history of China during the Common Era.

Multicentennial-scale temperature variations captured in the Tiancai Lake record are potentially related to variations in solar forcing and volcanic activity. The correspondence between the three highest magnitude cold events recorded at Tiancai Lake (250–310 AD, 570–650 AD and 1800–1823 AD) and times when solar minima coincided with periods of frequent volcanic eruptions, supports this explanation. However, we note that not all solar minima and/or times with frequent volcanic activity correspond with cold events in our record. Since the postindustrial period, the abrupt increase in temperature suggests that GHGs have become the major driving force on MAAT in this region.

The large-magnitude temperature variations shown in our record, consistent with instrumental data and existing paleoclimatic records on the Tibetan Plateau, suggest amplified temperature response in high elevation regions, possibly due to non-linear radiative feedbacks involving seasonal snow cover, clouds, water vapor, and aerosols. Furthermore, the Tiancai Lake record indicates a relatively cold climate during most of the first millennium, which appears to have been a feature of the Tibetan Plateau that is not seen globally, and potentially reflects a climate history unique to high-elevation areas. Finally, our record reveals that post-1989 AD warmth is greater than at any other time during the past 2000 years.

Acknowledgements

We thank S. Gao from Key Laboratory of Tibetan Environment Changes and Land Surface Processes, Institute of Tibetan Plateau Research, Chinese Academy of Sciences for LC-MS maintenance. This research was supported by the Program of Global Change and Mitigation, Ministry of Science and Technology of the People's Republic of China (#2016YFA0600502), the Strategic Priority Research Program of Chinese Academy of Sciences (#XDA2009000004), National Natural Science Foundation of China (#41877293, #41472315) and the China Scholarship Council (CSC).

W.J.D. would like to acknowledge support from the Vetlesen Foundation.

Appendix A. Supplementary material

Supplementary material related to this article can be found online at https://doi.org/10.1016/j.epsl.2018.12.028.

References

Appleby, P.G., 2002. Chronostratigraphic techniques in recent sediments. In: Tracking Environmental Change Using Lake Sediments. Springer, pp. 171–203.

Blaauw, M., Christen, J.A., 2011. Flexible paleoclimate age-depth models using an autoregressive gamma process. Bayesian Anal. 6, 457–474. https://doi.org/10.1214/11-BA618.

Chen, D.L., Xu, B.Q., Yao, T.D., Guo, Z.T., Cui, P., Chen, F.H., Zhang, R.H., Zhang, X.Z., Zhang, Y.L., Fan, J., Hou, Z.Q., Zhang, T.H., 2015. Assessment of past, present and future environmental changes on the Tibetan Plateau. Chin. Sci. Bull. 2015. https://doi.org/10.1360/N972014-01370.

Chu, K.-C., 1973. A preliminary study on the climatic fluctuations during the last 5000 years in China. Sci. Ser. 16, 226–256.

Cook, E.R., Krusic, P.J., Anchukaitis, K.J., Buckley, B.M., Nakatsuka, T., Sano, M., 2013. Tree-ring reconstructed summer temperature anomalies for temperate East Asia since 800 C.E. Clim. Dyn. 41, 2957–2972. https://doi.org/10.1007/s00382-012-1611-x.

Crowley, T.J., 2000. Causes of climate change over the past 1000 years. Science 289, 270–277. https://doi.org/10.1126/science.289.5477.270.

Dang, X., Ding, W., Yang, H., Pancost, R.D., Naafs, B.D.A., Xue, J., Lin, X., Lu, J., Xie, S., 2018. Different temperature dependence of the bacterial brGDGT isomers in 35 Chinese lake sediments compared to that in soils. Org. Geochem. 119, 72–79. https://doi.org/10.1016/j.orggeochem.2018.02.008.

De Jonge, C., Hopmans, E.C., Stadnitskaia, A., Rijpstra, W.I.C., Hofland, R., Tegelaar, E., Sinninghe Damsté, J.S., 2013. Identification of novel penta- and hexamethylated branched glycerol dialkyl glycerol tetraethers in peat using HPLC-MS2, GC-MS and GC-SMB-MS. Org. Geochem. 54, 78–82. https://doi.org/10.1016/j.orggeochem.2012.10.004.

De Jonge, C., Hopmans, E.C., Zell, C.I., Kim, J.-H., Schouten, S., Sinninghe Damsté, J.S., 2014a. Occurrence and abundance of 6-methyl branched glycerol dialkyl glycerol tetraethers in soils: implications for palaeoclimate reconstruction. Geochim. Cosmochim. Acta 141, 97–112. https://doi.org/10.1016/j.gca.2014.06.013.

De Jonge, C., Stadnitskaia, A., Hopmans, E.C., Cherkashov, G., Fedotov, A., Sinninghe Damsté, J.S., 2014b. In situ produced branched glycerol dialkyl glycerol tetraethers in suspended particulate matter from the Yenisei River, Eastern Siberia. Geochim. Cosmochim. Acta 125, 476–491. https://doi.org/10.1016/j.gca.2013.10.031.

Diaz, H.F., Trigo, R., Hughes, M.K., Mann, M.E., Xoplaki, E., Barriopedro, D., 2011. Spatial and temporal characteristics of climate in medieval times revisited. Bull. Am. Meteorol. Soc. 92, 1487–1500. https://doi.org/10.1175/BAMS-D-10-05003.1.

Dieffenbacher-Krall, A.C., Vandergoes, M.J., Denton, G.H., 2007. An inference model for mean summer air temperatures in the Southern Alps, New Zealand, using subfossil chironomids. Quat. Sci. Rev. 26, 2487–2504. https://doi.org/10.1016/j.quascirev.2007.06.016.

Foster, L.C., Pearson, E.J., Juggins, S., Hodgson, D.A., Saunders, K.M., Verleyen, E., Roberts, S.J., 2016. Development of a regional glycerol dialkyl glycerol tetraether (GDGT)—temperature calibration for Antarctic and sub-Antarctic lakes. Earth Planet. Sci. Lett. 433, 370–379. https://doi.org/10.1016/j.epsl.2015.11.018.

Ge, Q., Hao, Z., Zheng, J., Shao, X., 2013a. Temperature changes over the past 2000 yr in China and comparison with the Northern Hemisphere. Clim. Past 9, 1153–1160. https://doi.org/10.5194/cp-9-1153-2013.

Ge, Q., Zheng, J., Hao, Z., Liu, H., 2013b. General characteristics of climate changes during the past 2000 years in China. Sci. China Earth Sci. 56, 321–329. https://doi.org/10.1007/s11430-012-4370-y.

Gennaretti, F., Arseneault, D., Nicault, A., Perreault, L., Begin, Y., 2014. Volcano-induced regime shifts in millennial tree-ring chronologies from northeastern North America. Proc. Natl. Acad. Sci. 111, 10077–10082. https://doi.org/10.1073/pnas.1324220111.

Günther, F., Thiele, A., Gleixner, G., Xu, B., Yao, T., Schouten, S., 2014. Distribution of bacterial and archaeal ether lipids in soils and surface sediments of Tibetan lakes: implications for GDGT-based proxies in saline high mountain lakes. Org. Geochem. 67, 19–30. https://doi.org/10.1016/j.orggeochem.2013.11.014.

He, Y., Liu, W., Zhao, C., Wang, Z., Wang, H., Liu, Y., Qin, X., Hu, Q., An, Z., Liu, Z., 2013. Solar influenced late Holocene temperature changes on the northern Tibetan Plateau. Chin. Sci. Bull. 58, 1053–1059. https://doi.org/10.1007/s11434-012-5619-8.

Hegerl, G., Luterbacher, J., González-Rouco, F., Tett, S.F.B., Crowley, T., Xoplaki, E., 2011. Influence of human and natural forcing on European seasonal temperatures. Nat. Geosci. 4, 99–103. https://doi.org/10.1038/ngeo1057.

Hocking, R.R., 1976. A biometrics invited paper. The analysis and selection of variables in linear regression. Biometrics 32, 1. https://doi.org/10.2307/2529336.

Jones, P.D., Mann, M.E., 2004. Climate over past millennia. Rev. Geophys. 42, RG2002. https://doi.org/10.1029/2003RG000143.

Kassambara, A., 2016. Ggcorrplot. CRAN. https://cran.rproject.org/web/packages/ggcorrplot/index.html.

Lau, W.K.M., Kim, M.-K., Kim, K.-M., Lee, W.-S., 2010. Enhanced surface warming and accelerated snow melt in the Himalayas and Tibetan Plateau induced by absorbing aerosols. Environ. Res. Lett. 5, 025204. https://doi.org/10.1088/1748-9326/5/2/025204.

Li, J., Pancost, R.D., Naafs, B.D.A., Yang, H., Zhao, C., Xie, S., 2016. Distribution of glycerol dialkyl glycerol tetraether (GDGT) lipids in a hypersaline lake system. Org. Geochem. 99, 113–124. https://doi.org/10.1016/j.orggeochem.2016.06.007.

Li, Z., He, Y., Wang, C., Wang, X., Xin, H., Zhang, W., Cao, W., 2011. Spatial and temporal trends of temperature and precipitation during 1960–2008 at the Hengduan Mountains, China. Quat. Int. 236, 127–142. https://doi.org/10.1016/j.quaint.2010.05.017.

Liu, X., Chen, B., 2000. Climatic warming in the Tibetan Plateau during recent decades. Int. J. Climatol. 20, 1729–1742.

Ljungqvist, F.C., 2010. A new reconstruction of temperature variability in the extra-tropical Northern Hemisphere during the last two millennia. Geogr. Ann., Ser. A, Phys. Geogr. 92, 339–351. https://doi.org/10.1111/j.1468-0459.2010.00399.x.

Loomis, S.E., Russell, J.M., Ladd, B., Street-Perrott, F.A., Sinninghe Damsté, J.S., 2012. Calibration and application of the branched GDGT temperature proxy on East African lake sediments. Earth Planet. Sci. Lett. 357–358, 277–288. https://doi.org/10.1016/j.epsl.2012.09.031.

Loomis, S.E., Russell, J.M., Eggermont, H., Verschuren, D., Damsté, J.S.S., 2014. Effects of temperature, pH and nutrient concentration on branched GDGT distributions in East African lakes: implications for paleoenvironmental reconstruction. Org. Geochem. 66, 25–37. https://doi.org/10.1016/j.orggeochem.2013.10.012.

Mann, M.E., Zhang, Z., Rutherford, S., Bradley, R.S., Hughes, M.K., Shindell, D., Ammann, C., Faluvegi, G., Ni, F., 2009. Global signatures and dynamical origins of the Little Ice Age and medieval climate anomaly. Science 326, 1256–1260. https://doi.org/10.1126/science.1177303.

Moberg, A., Sonechkin, D.M., Holmgren, K., Datsenko, N.M., Karlén, W., 2005. Highly variable Northern Hemisphere temperatures reconstructed from low- and high-resolution proxy data. Nature 433, 613–617. https://doi.org/10.1038/nature03265.

Naafs, B.D.A., Gallego-Sala, A.V., Inglis, G.N., Pancost, R.D., 2017a. Refining the global branched glycerol dialkyl glycerol tetraether (brGDGT) soil temperature calibration. Org. Geochem. 106, 48–56. https://doi.org/10.1016/j.orggeochem.2017.01.009.

Naafs, B.D.A., Inglis, G.N., Zheng, Y., Amesbury, M.J., Biester, H., Bindler, R., Blewett, J., Burrows, M.A., del Castillo Torres, D., Chambers, F.M., Cohen, A.D., Evershed, R.P., Feakins, S.J., Gałka, M., Gallego-Sala, A., Gandois, L., Gray, D.M., Hatcher, P.G., Honorio Coronado, E.N., Hughes, P.D.M., Huguet, A., Könönen, M., Laggoun-Défarge, F., Lähteenoja, O., Lamentowicz, M., Marchant, R., McClymont, E., Pontevedra-Pombal, X., Ponton, C., Pourmand, A., Rizzuti, A.M., Rochefort, L., Schellekens, J., De Vleeschouwer, F., Pancost, R.D., 2017b. Introducing global peat-specific temperature and pH calibrations based on brGDGT bacterial lipids. Geochim. Cosmochim. Acta 208, 285–301. https://doi.org/10.1016/j.gca.2017.01.038.

PAGES 2k Consortium, 2013. Continental-scale temperature variability during the past two millennia. Nat. Geosci. 6, 339–346. https://doi.org/10.1038/ngeo1797.

PAGES 2k Consortium, 2017. A global multiproxy database for temperature reconstructions of the Common Era. Sci. Data 4, 170088. https://doi.org/10.1038/sdata.2017.88.

Pearson, E.J., Juggins, S., Talbot, H.M., Weckström, J., Rosén, P., Ryves, D.B., Roberts, S.J., Schmidt, R., 2011. A lacustrine GDGT-temperature calibration from the Scandinavian Arctic to Antarctic: renewed potential for the application of GDGT-paleothermometry in lakes. Geochim. Cosmochim. Acta 75, 6225–6238. https://doi.org/10.1016/j.gca.2011.07.042.

Pepin, N., Bradley, R.S., Diaz, H.F., Baraer, M., Caceres, E.B., Forsythe, N., Fowler, H., Greenwood, G., Hashmi, M.Z., Liu, X.D., Miller, J.R., Ning, L., Ohmura, A., Palazzi, E., Rangwala, I., Schöner, W., Severskiy, I., Shahgedanova, M., Wang, M.B., Williamson, S.N., Yang, D.Q., 2015. Elevation-dependent warming in mountain regions of the world. Nat. Clim. Change 5, 424–430. https://doi.org/10.1038/nclimate2563.

Peterse, F., van der Meer, J., Schouten, S., Weijers, J.W.H., Fierer, N., Jackson, R.B., Kim, J.-H., Sinninghe Damsté, J.S., 2012. Revised calibration of the MBT–CBT paleotemperature proxy based on branched tetraether membrane lipids in surface soils. Geochim. Cosmochim. Acta 96, 215–229. https://doi.org/10.1016/j.gca.2012.08.011.

Rangwala, I., Miller, J.R., Xu, M., 2009. Warming in the Tibetan Plateau: possible influences of the changes in surface water vapor. Geophys. Res. Lett. 36. https://doi.org/10.1029/2009GL037245.

Reimer, P.J., Bard, E., Bayliss, A., Beck, J.W., Blackwell, P.G., Ramsey, C.B., Buck, C.E., Cheng, H., Edwards, R.L., Friedrich, M., Grootes, P.M., Guilderson, T.P., Haflidason, H., Hajdas, I., Hatté, C., Heaton, T.J., Hoffmann, D.L., Hogg, A.G., Hughen, K.A., Kaiser, K.F., Kromer, B., Manning, S.W., Niu, M., Reimer, R.W., Richards, D.A., Scott, E.M., Southon, J.R., Staff, R.A., Turney, C.S.M., van der Plicht, J., 2013. IntCal13 and Marine13 radiocarbon age calibration curves 0–50,000 years cal BP. Radiocarbon 55, 1869–1887. https://doi.org/10.2458/azu_js_rc.55.16947.

Russell, J.M., Hopmans, E.C., Loomis, S.E., Liang, J., Sinninghe Damsté, J.S., 2018. Distributions of 5- and 6-methyl branched glycerol dialkyl glycerol tetraethers (brGDGTs) in East African lake sediment: effects of temperature, pH, and new lacustrine paleotemperature calibrations. Org. Geochem. 117, 56–69. https://doi.org/10.1016/j.orggeochem.2017.12.003.

Shi, F., Ge, Q., Yang, B., Li, J., Yang, F., Ljungqvist, F.C., Solomina, O., Nakatsuka, T., Wang, N., Zhao, S., Xu, C., Fang, K., Sano, M., Chu, G., Fan, Z., Gaire, N.P., Zafar, M.U., 2015. A multi-proxy reconstruction of spatial and temporal variations in Asian summer temperatures over the last millennium. Clim. Change 131, 663–676. https://doi.org/10.1007/s10584-015-1413-3.

Sigl, M., Winstrup, M., McConnell, J.R., Welten, K.C., Plunkett, G., Ludlow, F., Büntgen, U., Caffee, M., Chellman, N., Dahl-Jensen, D., Fischer, H., Kipfstuhl, S., Kostick, C., Maselli, O.J., Mekhaldi, F., Mulvaney, R., Muscheler, R., Pasteris, D.R., Pilcher, J.R., Salzer, M., Schüpbach, S., Steffensen, J.P., Vinther, B.M., Woodruff, T.E., 2015. Timing and climate forcing of volcanic eruptions for the past 2500 years. Nature 523, 543–549. https://doi.org/10.1038/nature14565.

Sinninghe Damsté, J.S., Ossebaar, J., Abbas, B., Schouten, S., Verschuren, D., 2009. Fluxes and distribution of tetraether lipids in an equatorial African lake: constraints on the application of the TEX86 palaeothermometer and BIT index in lacustrine settings. Geochim. Cosmochim. Acta 73, 4232–4249. https://doi.org/10.1016/j.gca.2009.04.022.

Sinninghe Damsté, J.S., Rijpstra, W.I.C., Hopmans, E.C., Weijers, J.W.H., Foesel, B.U., Overmann, J., Dedysh, S.N., 2011. 13,16-Dimethyl octacosanedioic acid (iso-diabolic acid), a common membrane-spanning lipid of Acidobacteria subdivisions 1 and 3. Appl. Environ. Microbiol. 77, 4147–4154. https://doi.org/10.1128/AEM.00466-11.

Steinhilber, F., Abreu, J.A., Beer, J., Brunner, I., Christl, M., Fischer, H., Heikkilä, U., Kubik, P.W., Mann, M., McCracken, K.G., 2012. 9,400 years of cosmic radiation and solar activity from ice cores and tree rings. Proc. Natl. Acad. Sci. 109, 5967–5971. https://doi.org/10.1073/pnas.1118965109.

Stocker, et al. (Eds.), 2013. Climate Change 2013: The Physical Science Basis. Contribution of Working Group I to the Fifth Assessment Report of the Intergovernmental Panel on Climate Change. Cambridge University Press, Cambridge, United Kingdom and New York, NY, USA.

Sun, Q., Chu, G., Liu, M., Xie, M., Li, S., Ling, Y., Wang, X., Shi, L., Jia, G., Lü, H., 2011. Distributions and temperature dependence of branched glycerol dialkyl glycerol tetraethers in recent lacustrine sediments from China and Nepal. J. Geophys. Res. 116. https://doi.org/10.1029/2010JG001365.

Tierney, J.E., Russell, J.M., 2009. Distributions of branched GDGTs in a tropical lake system: implications for lacustrine application of the MBT/CBT paleoproxy. Org. Geochem. 40, 1032–1036. https://doi.org/10.1016/j.orggeochem.2009.04.014.

Tierney, J.E., Russell, J.M., Eggermont, H., Hopmans, E.C., Verschuren, D., Sinninghe Damsté, J.S., 2010. Environmental controls on branched tetraether lipid distributions in tropical East African lake sediments. Geochim. Cosmochim. Acta 74, 4902–4918. https://doi.org/10.1016/j.gca.2010.06.002.

Wang, Q., Fan, X., Wang, M., 2014. Recent warming amplification over high elevation regions across the globe. Clim. Dyn. 43, 87–101. https://doi.org/10.1007/s00382-013-1889-3.

Weber, Y., De Jonge, C., Rijpstra, W.I.C., Hopmans, E.C., Stadnitskaia, A., Schubert, C.J., Lehmann, M.F., Sinninghe Damsté, J.S., Niemann, H., 2015. Identification and carbon isotope composition of a novel branched GDGT isomer in lake sediments: evidence for lacustrine branched GDGT production. Geochim. Cosmochim. Acta 154, 118–129. https://doi.org/10.1016/j.gca.2015.01.032.

Weijers, J.W.H., Schouten, S., Hopmans, E.C., Geenevasen, J.A.J., David, O.R.P., Coleman, J.M., Pancost, R.D., Sinninghe Damste, J.S., 2006. Membrane lipids of mesophilic anaerobic bacteria thriving in peats have typical archaeal traits. Environ. Microbiol. 8, 648–657. https://doi.org/10.1111/j.1462-2920.2005.00941.x.

Weijers, J.W.H., Schouten, S., van den Donker, J.C., Hopmans, E.C., Sinninghe Damsté, J.S., 2007. Environmental controls on bacterial tetraether membrane lipid distribution in soils. Geochim. Cosmochim. Acta 71, 703–713. https://doi.org/10.1016/j.gca.2006.10.003.

Wiles, G.C., D'Arrigo, R.D., Villalba, R., Calkin, P.E., Barclay, D.J., 2004. Century-scale solar variability and Alaskan temperature change over the past millennium. Geophys. Res. Lett. 31. https://doi.org/10.1029/2004GL020050.

Xiao, X., Haberle, S.G., Shen, J., Yang, X., Han, Y., Zhang, E., Wang, S., 2014. Latest Pleistocene and Holocene vegetation and climate history inferred from an Alpine lacustrine record, northwestern Yunnan Province, southwestern China. Quat. Sci. Rev. 86, 35–48. https://doi.org/10.1016/j.quascirev.2013.12.023.

Yan, L., Liu, X., 2014. Has climatic warming over the Tibetan Plateau paused or continued in recent years. J. Earth Ocean Atmos. Sci. 1, 13–28.

Yang, B., Achim, B., Shi, Y.F., 2003. Late Holocene temperature fluctuations on the Tibetan Plateau. Quat. Sci. Rev. 22, 2335–2344. https://doi.org/10.1016/S0277-3791(03)00132-X.

Yang, Y.D., 2005. Monsoon Climate Change and Disasters in Yunnan Province During the Qing Dynasty (1711–1911). Dissertation (PhD). Fudan University, Shanghai, China (in Chinese).

Zhang, D., Jim, C.Y., Lin, C.S., He, Y.Q., Lee, F., 2005. Climate change, social unrest and dynastic transition in ancient China. Chin. Sci. Bull. 50, 137–144. https://doi.org/10.1360/03wd0641.

Zhang, E., Chang, J., Cao, Y., Sun, W., Shulmeister, J., Tang, H., Langdon, P.G., Yang, X., Shen, J., 2017. Holocene high-resolution quantitative summer temperature reconstruction based on subfossil chironomids from the southeast margin of the Qinghai–Tibetan Plateau. Quat. Sci. Rev. 165, 1–12. https://doi.org/10.1016/j.quascirev.2017.04.008.

Zhang, Z., Tian, H., Cazelles, B., Kausrud, K.L., Brauning, A., Guo, F., Stenseth, N.C., 2010. Periodic climate cooling enhanced natural disasters and wars in China during AD 10–1900. Proc. R. Soc. B, Biol. Sci. 277, 3745–3753. https://doi.org/10.1098/rspb.2010.0890.